Numerical prediction of the boundary layers in the flow around a cylinder using a fixed velocity field

P. Wapperom * and M. Renardy

Dept. of Mathematics, Virginia Tech, Blacksburg, VA 24061-0123, USA

Abstract

For the flow around a cylinder of an upper convected Maxwell or Oldroyd-B fluid, thin stress boundary layers develop close to the cylinder wall and in the wake. Numerical simulations of this flow problem already fail to converge at a Weissenberg number of order unity. For the boundary layer and in the wake, high-Weissenberg number stress scalings, using a given, Newtonian velocity field have been predicted by Renardy (J. Non-Newtonian Fluid Mech. 90 (2000) 13–23). We develop a purely Lagrangian technique that is able to resolve thin stress boundary layers in an accurate and very efficient manner up to arbitrarily large Weissenberg numbers. This is in sharp contrast with a traditional method which has severe difficulties in predicting the correct solution at relatively low Weissenberg numbers and suffers from long computational times. With the purely Lagrangian technique, we observe numerically the existence of thin regions with large stresses, just outside the boundary layer along the cylinder and birefringent strand in the wake, just as predicted by the asymptotic analysis. All theoretical scalings are observed at larger values of the Weissenberg number than can be reached in the benchmark flow around a cylinder with non-fixed kinematics. Around the cylinder, the asymptotic results already appear to be valid at moderate values of the Weisenberg number. In the wake very large Weissenberg numbers are necessary to observe stresses that are proportional to We^5.

Key words: Boundary layers, Cylinder, High Weissenberg asymptotics, Upper-Convected Maxwell model, Numerical simulation

* Corresponding author.
Email address: wapperom@math.vt.edu (P. Wapperom).

1 Introduction

One of the classical benchmark flows in the numerical simulation of viscoelastic fluids is the flow of an upper convected Maxwell (UCM) or Oldroyd-B fluid around a cylinder confined between two parallel plates. The problem is well suited as a benchmark problem for understanding the flow of viscoelastic liquids in complex geometries. Near the cylinder both shearing and extensional effects are present, near the channel walls and in the gap between the channel walls and cylinders the flow is primarily a shear flow, and near the axis of symmetry the flow is dominated by extension. The geometry of this benchmark problem is relatively simple and it has no singularities as for example the flow through a contraction with sharp corner. However, producing converged and accurate numerical results for stresses and velocities is a very challenging task due to the presence of the upstream and downstream stagnation points, the thin stress boundary layer near the cylinder, and the birefringent strand in the wake of the cylinder. The maximum Weissenberg number (based on the average velocity and cylinder radius) at which numerical simulations are successful is around 1. Despite the absence of singularities, these values of Weissenberg numbers are the lowest of all benchmark flows. The flow around a cylinder between parallel plates is, for example, numerically also more difficult than the corresponding problem of a sphere in a tube, for which converged solutions for Weissenberg numbers of $We = 2$ to $We = 2.5$ are reported.

Practically all usual grid-based methods have been applied to the flow around a cylinder of the UCM and Oldroyd-B fluid, for example [1–8]. Various methods now seem to predict similar drag factors on the cylinder wall and converged solutions at a given mesh are reported up to approximately $We \approx 1 - 1.2$. A recent comparison of drag factors obtained with various numerical techniques is given in Owens and Phillips [9]. As pointed out by several authors, for example [10,2], the drag coefficient is a poor indicator of the quality of the solution. Convergent drag factors do not imply that the numerical solution has converged with mesh refinement on the whole flow domain. Most critical seems to be the stress field in the wake of the cylinder where steep stress gradients develop at relatively low Weissenberg numbers of about 0.7. Careful studies of the stress profiles in the wake are, however, suspiciously rare [7]. We discuss briefly the most recent findings on very refined meshes. Owens et al. [8] used a spectral technique with local upwinding. They found a converging trend for the stress in the wake of an Oldroyd-B fluid at $We = 0.7$ while for Weissenberg numbers of 0.8 and higher such a trend could not be observed. These results agree well with those of the Galerkin/least-square finite element method of Fan et al. [2]. Furthermore, for the UCM fluid these authors observed a converging trend for the stress in the wake at $We = 0.6$ while this trend was absent at $We = 0.75$. Alves et al. [5] used a finite volume method in combination with very refined meshes. They showed that only for the most refined mesh in the

wake of the cylinder, the stresses in the wake agree well with those of [2], both for the UCM and the Oldroyd-B fluid. For the Oldroyd-B fluid, stress profiles in the wake are given up to a Weissenberg number of 1 at which the maximum stress has increased about a factor of three compared to $We = 0.7$. Caola et al. [6] performed simulations for the Oldroyd-B fluid with a DEVSS-G/DG finite element discretisation. They report convergence to a steady state solution at $We = 1$ on a very refined mesh with a smallest element size of the order of 10^{-3} near the rear stagnation point. Unfortunately, the authors of [5] and [6] have not established whether the stress in the wake converges with mesh refinement at $We = 1$. The longitudinal normal stress in the wake of the cylinder found in [6] seems to be considerably lower than in [5].

The reason why numerical simulations of the benchmark flow of a UCM or Oldroyd-B fluid around a cylinder (with non-fixed kinematics) fail to converge is currently not well understood. All accurate numerical techniques currently break down at Weissenberg numbers around 1. Fan et al. [2] and Owens et al. [8], for example, speculated that numerical solutions for the flow of an Oldroyd-B fluid at Weissenberg numbers higher than about 0.8 are probably numerical artifacts. Caola et al. [6] used very fine meshes and couldn't reach a steady state for their simulations above $We = 1$. They suggested, however, that the instability is numerical and that even their very refined meshes were not able to resolve the steep stress gradients in the wake of the cylinder. Dou and Phan-Thien [4] have suggested that the flow near the front stagnation point might be a source of numerical difficulty. Whether solutions do not exist or whether currently used meshes are not able to resolve the boundary layers is difficult to establish from numerical simulations of the benchmark flow with non-fixed kinematics. As long as little is known about the mathematical structure of the boundary layers and current mathematical techniques fail to converge this will remain an open question. This is unsatisfactory.

The flow of a UCM fluid around a cylinder is a very interesting benchmark problem for a second reason. In case fixed, Newtonian kinematics are assumed, there is no doubt about the existence of a solution, while the numerical computation is still a challenging task. Asymptotical analysis [11] predicts a thin stress boundary layer near the cylinder wall and a thin birefringent strand in the wake, as observed in numerical simulations of the benchmark flow. On the other hand the introduction of a fixed Newtonian velocity field introduces of course quantitative differences with the benchmark flow around a cylinder. The velocity field obtained for an Oldroyd-B fluid at maximum attainable Weissenberg numbers of order unity [5] are, however, still very similar to the Newtonian velocity field. More specifically, no recirculation zones are observed and the most striking difference is a slight shift in the streamlines downstream of the cylinder. For the stress boundary layers, only the streamlines that pass close to the cylinder wall are relevant. For such streamlines, the only noticeable difference is a small shift in the close vicinity of the rear stagnation point.

Such streamline patterns will predict, in combination with the two stagnation points, qualitatively similar stress boundary layers as in [11].

In this paper we present accurate numerical solutions for the flow around a cylinder in a fixed, Newtonian-like velocity field, which we define in Section 2. The computations are performed with a Lagrangian technique that we discuss in Section 3 and validate in Section 4. Then, in Section 5 we establish numerically the range of Weissenberg numbers for which the asymptotical scalings are valid. We show that using a Lagrangian technique, it is possible to observe all high-Weissenberg number scalings predicted in [11]. Some scalings, however, are only observed at very high Weissenberg numbers. Particularly the scalings in the wake occur at much higher Weissenberg numbers than can currently be attained in the benchmark flow with non-fixed kinematics. A comparison with the asymptotic scalings at Weissenberg numbers of the order one as in [5,6] is therefore useless. We show that the asymptotical scalings are only observed at Weissenberg numbers that are 1 to 2 orders of magnitude higher, far beyond the physical applicability of the UCM and Oldroyd-B model. In the discussion in Section 6 we indicate how the flow around a cylinder with fixed kinematics and the proposed Lagrangian numerical technique can be used by other computational groups to verify and improve simulations for the benchmark flow with non-fixed kinematics.

2 Problem description

A classical benchmark problem for viscoelastic flows is the flow around a cylinder in a confined geometry. The constitutive equation that is most frequently considered is the upper-convected Maxwell (UCM) model. The UCM model in non-dimensional form consists of an evolution equation for the configuration tensor $\boldsymbol{b}$ which is related to the extra-stress tensor $\boldsymbol{T}$ by a simple algebraic equation,

$$\frac{D\boldsymbol{b}}{Dt} = (\nabla \boldsymbol{v})^T \cdot \boldsymbol{b} + \boldsymbol{b} \cdot \nabla \boldsymbol{v} - \frac{1}{We}\left(\boldsymbol{b} - \boldsymbol{I}\right), \tag{1}$$

$$\boldsymbol{T} = \frac{1}{We}(\boldsymbol{b} - \boldsymbol{I}), \tag{2}$$

where D/Dt represents the material derivative, $\nabla \boldsymbol{v}$ the velocity gradient, and $\boldsymbol{I}$ the unit tensor.

For the flow around a cylinder using a fixed velocity field that fulfills the essential characteristics of a Newtonian velocity field, asymptotic scalings are known for high Weissenberg numbers [11]. To perform the asymptotical analysis, the stress was expressed in a basis which is aligned with the velocity field

with stress components λ, μ, and ν,

$$\boldsymbol{T} = \frac{1}{We}(\boldsymbol{b} - \boldsymbol{I}) = \lambda \boldsymbol{v}\boldsymbol{v}^T + \mu\left(\boldsymbol{v}\boldsymbol{w}^T + \boldsymbol{w}\boldsymbol{v}^T\right) + \nu \boldsymbol{w}\boldsymbol{w}^T, \tag{3}$$

where $\boldsymbol{w}$ is a vector perpendicular to the velocity vector $\boldsymbol{v} = (u, v)$,

$$\begin{aligned} \boldsymbol{w} &= \left(-\frac{v}{u^2+v^2}, \frac{u}{u^2+v^2}\right), \\ \boldsymbol{w} \cdot \boldsymbol{w} &= \frac{1}{u^2+v^2}. \end{aligned} \tag{4}$$

The coefficients λ, μ and ν can be expressed in the components of the configuration tensor $\boldsymbol{b}$ by

$$\begin{aligned} \lambda &= \frac{1}{We}\frac{(b_{11}-1)u^2 + 2b_{12}uv + (b_{22}-1)v^2}{(u^2+v^2)^2}, \\ \mu &= \frac{1}{We}\frac{(b_{22}-b_{11})uv + b_{12}(u^2-v^2)}{u^2+v^2}, \\ \nu &= \frac{1}{We}\left[(b_{11}-1)v^2 - 2b_{12}uv + (b_{22}-1)u^2\right]. \end{aligned} \tag{5}$$

Asymptotical analysis predicts a thin boundary layer with large stresses near the cylinder wall and a thin birefringent strand in the wake of the cylinder where the stress component λ is of the order We^3. Just outside the boundary layer and birefringent strand, however, very thin regions develop where λ is much larger. There, λ is of the order We^5. Close to the cylinder, $|\boldsymbol{v}|$ is of the order We^{-1} which results in viscoelastic stresses of order We^3. In the wake, however, $|\boldsymbol{v}|$ is of order 1 which results in viscoelastic stresses of order We^5. The scalings of the stress components λ, μ, and ν are summarized in Fig. 1. The origin of these large stresses is in the stretching flow near the upstream stagnation point. Henceforth, we will call these regions high stress regions to distinguish them from the boundary layer and birefringent strand. The high stress region along the cylinder and in the wake occurs at stream function values of the order We^{-2}.

The asymptotical analysis in [11] was performed using a fixed velocity field that has the characteristics of a Newtonian velocity field. Rather than solving the Newtonian velocity field numerically and using it to compute the stresses, we construct a velocity field that fulfills the essential requirements near the cylinder. This facilitates comparison of results obtained from numerical simulations using the configuration tensor with the coefficients λ, μ, and ν used in the asymptotical analysis. Since the denominator in Eq. (5) contains a term

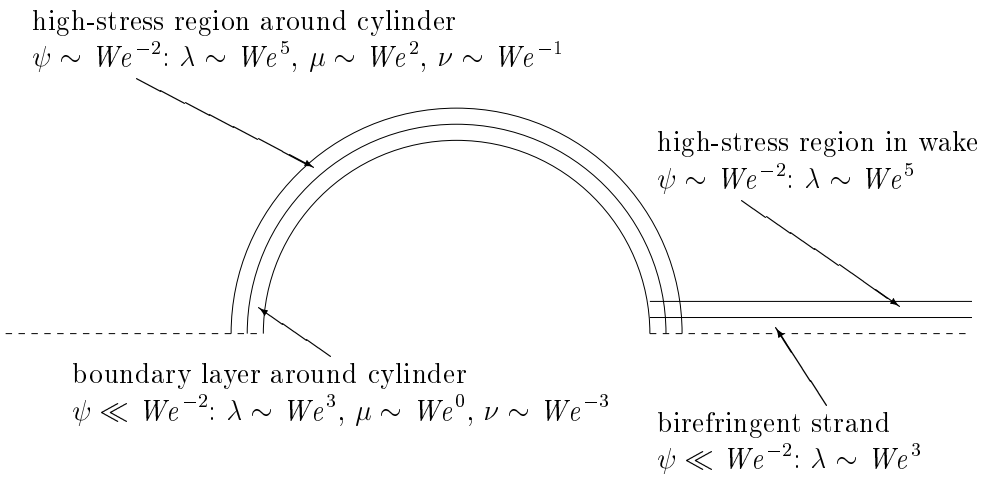

Fig. 1. Boundary layer, birefringent strand, and high-stress regions along the cylinder and in the wake with corresponding scalings of stress components λ, μ, and ν.

$(u^2+v^2)^2$, small numerical errors can have a dramatic impact on the resulting stress coefficient λ when the velocities are small.

A stream function that fulfills the necessary requirements near the cylinder is

$$\psi = y\left(1 - \frac{1}{x^2+y^2}\right)^2. \tag{6}$$

The streamlines obtained from Eq. (6) near the cylinder are depicted in Fig. 2. Although these streamlines are not identical to those of the benchmark flow

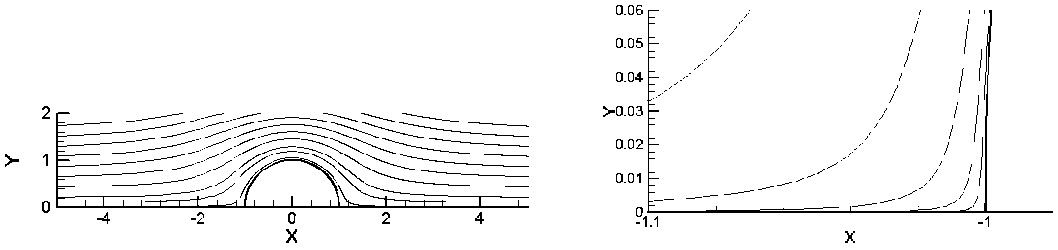

Fig. 2. Streamlines near the cylinder obtained from Eq. (6); (a) stream function values 10^{-2}, 10^{-1}, and $2\cdot10^{-1}+2k\cdot10^{-1}$ for $k=0,\ldots,7$, (b) zoom at the upstream stagnation point with $\psi = 10^{-3}$, 10^{-4}, 10^{-5}, 10^{-6}

with non-fixed kinematics, they agree qualitatively with streamline patterns up to the limiting Weissenberg number of 0.9 for an Oldroyd-B fluid (see Fig. 19 in [5]). Both do not show vortices and for streamlines passing close to the cylinder only small quantitative differences are apparent near the downstream stagnation point.

The velocities corresponding to the stream function Eq. (6) are

$$u = 4y^2\frac{x^2+y^2-1}{(x^2+y^2)^3} + \left(1-\frac{1}{x^2+y^2}\right)^2,$$
$$v = -4xy\frac{x^2+y^2-1}{(x^2+y^2)^3} \tag{7}$$

and the velocity gradient has components

$$\frac{\partial u}{\partial x} = \frac{4x(x^4+5y^2-3y^4-x^2(1+2y^2))}{(x^2+y^2)^4},$$
$$\frac{\partial u}{\partial y} = \frac{4y(3x^4-y^2(y^2-3)+x^2(2y^2-3))}{(x^2+y^2)^4},$$
$$\frac{\partial v}{\partial x} = \frac{4y(3x^4+y^2-y^4+x^2(2y^2-5))}{(x^2+y^2)^4},$$
$$\frac{\partial v}{\partial y} = -\frac{4x(x^4+5y^2-3y^4-x^2(1+2y^2))}{(x^2+y^2)^4}. \tag{8}$$

We note that for $x \to \pm\infty$ the velocities reduce to $u = 1$ and $v = 0$. This differs from the Poiseuille flow in the benchmark flow around a cylinder and in the asymptotical analysis. As explained in [11], however, this difference is not relevant for the asymptotic behaviour.

Henceforth, we will focus on the most interesting regions, the boundary layer along the cylinder, the birefringent strand, and the high-stress regions close to the cylinder and in the wake.

3 Computational method

To solve the system of differential equations, we integrate along the fluid trajectories. The fluid trajectories are obtained by integrating $\partial \boldsymbol{x}/\partial t = \boldsymbol{v}$ with a fourth-order Runge–Kutta method as in [12,13]. The advantage of the velocity field, Eq. (7), is that it is known as at every location in the flow domain. This makes a finite element interpolation to obtain velocities at a certain location is unnecessary. Furthermore, an analytical expression for the velocity field makes it easy to restrict the computational domain to a relatively small region where steep stress gradients develop when we integrate along fluid trajectories.

The stresses are obtained by integrating the constitutive equation along a streamline using a predictor-corrector method. Here, the velocity gradients are calculated from Eq. (8). One major problem with viscoelastic computations

is that the determinant of the configuration model may become negative due to numerical errors. This may lead to spurious numerical results or blow-up of the solutions. For the UCM model, it is not possible to correct negative determinants in an ad hoc manner [14]. By using a transformation of variables [15], however, positive definiteness of the configuration tensor $\boldsymbol{b}$ can be ensured.

Since very large stress gradients develop in the thin boundary layer along the cylinder and birefringent strand in the wake, it is crucial to have a sufficient resolution in both x and y-direction for plotting purposes. This means that we need a sufficient number of fluid trajectories and a sufficient number of data points on each trajectory.

In order to ensure an adequate number of data points along each trajectory, we have defined a grid in the x-direction. When a trajectory passes a grid coordinate in the x direction the stresses are recorded. We divide the x direction in 6 regions. The first is the inflow region which only contains low stresses but needs to be sufficiently long to prescribe zero stress boundary conditions at the inlet. We found that specifying zero stresses at $x = -50$ did not significantly change the results. In the inlet region, the solution is very smooth and the grid can be very coarse. The second region is just before the upstream stagnation point. Very close to the stagnation point very large stresses develop and a very fine mesh is taken. Regions 3 spans the cylinder from the stagnation point to the top of the cylinder. Since large gradients are present in this region, a fine mesh is needed to accurately represent the solution. However, the mesh can be gradually coarsened away from the stagnation point. Region 4 is the mirror of region 3, so that we have a very fine grid near the downstream stagnation point. Region 5 and 6 contain the wake of the cylinder. The grid is very fine near the upstream stagnation point and is gradually coarsened towards the exit, $x = 50$. This turns out to be sufficient to capture the gradients along the trajectories. The outlet at $x = 50$ has been chosen in such a way that a reasonable part of the birefringent strand and high-stress region in the wake is covered by the computational domain. Since no boundary conditions need to be specified at the exit, this has no impact on the obtained solution. Note that this is in contrast to the full problem when the momentum equations are solved simultaneously. Then a sufficient exit length has to be chosen in order to apply boundary conditions for the velocity.

The details of the grid in the x-direction are given in Table 1. We want to stress here that the above grid points in the x direction are only selected points along the trajectories used for postprocessing. The actual points used for the integration along a trajectory is much larger.

In order to guarantee a sufficient number of fluid trajectories in the thin regions with large stresses without using an excessive number of fluid trajectories, we define starting points of trajectories at the inlet by partitioning the range

region	I	II	III	IV	V	VI
x_{start}	-50	-2	-1	0	1	5
x_{end}	-2	-1	0	1	5	50
N	13	60	190	190	1200	200
l_{start}	$1.67 \cdot 10^{1}$	$1.0 \cdot 10^{-1}$	$2.0 \cdot 10^{-4}$	$2.5 \cdot 10^{-2}$	$2.0 \cdot 10^{-4}$	$1.5 \cdot 10^{-2}$
l_{end}	$1.0 \cdot 10^{-1}$	$2.0 \cdot 10^{-4}$	$2.5 \cdot 10^{-2}$	$2.0 \cdot 10^{-4}$	$1.5 \cdot 10^{-2}$	$9.4 \cdot 10^{-1}$

Table 1
Details of the grid in the x-coordinate for each region: x-coordinate of first point of each region x_{start}, x-coordinate of last point of each region x_{end}, number of intervals per region N, length of first interval in each region l_{start}, length of last interval in each region l_{end}.

of y-coordinates using a logarithmic scale. Since the stream function value is practically equal to the y coordinate at the inlet, this corresponds to the values of the stream function ψ. We consider trajectories between $y_{\min} = 10^{-10}$ and $y_{\max} = 10^{-1}$, which correspond to $\psi_{\min} \approx 10^{-10}$ and $\psi_{\max} \approx 10^{-1}$. The trajectories are defined by specifying equidistantly initial points of fluid trajectories on the interval $[\log y_{\min}, \log y_{\max}]$. For the computations we find that $y_{\min} = 10^{-10}$ and $y_{\max} = 10^{-1}$ is sufficient to identify the boundary layer, birefringent strand, and high-stress regions.

4 Validation of the method

Even though the constitutive equations for the stress are solved for a given velocity field, obtaining an accurate numerical solution is far from trivial. To verify the accuracy of our numerical technique, we have performed additional computations with Mathematica using a different numerical technique.

Before we validate the Lagrangian method described in Section 3, we want to stress the non-trivial character of the flow around a cylinder in a Newtonian velocity field by discussing the difficulties observed with the backward-tracking Lagrangian particle method (BLPM) [13] for this flow. For BLPM, the stress at a certain location is computed by tracking a fluid trajectory backwards in time over a single time step Δt, evaluating suitable initial values of the configuration tensor at that point, and then integrating forwards the evolution equation along the obtained trajectory. The main difference with the method discussed in Section 3 is the initilization step for BLPM, which consists of a biquadratic interpolation of stored nodal values at the previous time level. For the purely Lagrangian method, we only need to specify initial values at the inlet where the solution is very smooth. For both methods, we use a fourth-order Runge–Kutta technique to determine a fluid trajectory and a predictor–corrector scheme to

integrate the evolution equations along a trajectory. This requires the velocity and velocity gradient to be known at a priori unknown locations. For BLPM those quantities are obtained using a biquadratic interpolation from the nodal values. For the purely Lagrangian technique, we used Eqs. (7) and (8) for the velocity and velocity gradient, respectively.

Preliminary calculations with the real Newtonian velocity field, showed that, at low Weissenberg numbers, BLPM was able to predict the correct stresses at the cylinder wall and in the wake when the mesh was sufficiently fine. The most refined mesh contained we used had over 14,000 elements. For the asymptotic scalings to be valid, stresses need to be convected around the cylinder. Calculations performed using Mathematica for a single streamline revealed, however, that Weissenberg number between 16 and 32 were needed, which would require much finer meshes. In view of the significant simulation times encountered already for the relatively low Weissenberg number flows, 1 to 2 days, we decided to proceed differently. We used a mesh of 1 element wide between two streamlines with stream function $\psi = 2 \times 10^{-4}$ and $\psi = 2.5 \times 10^{-4}$ and used the approximate Newtonian velocity field instead. Then, the mesh between two streamlines can easily be constructed using Eq. (6). The first significant differences appeared at $We = 8$. Two meshes were used with 800 and over 1000 elements in the flow direction, with a minimum length of $6 \times 10^{-4} R$ and $2 \times 10^{-4} R$ in the flow direction, respectively. For both meshes, BLPM underpredicted the stress coefficient λ over a wide range of x-coordinates with a maximum of about 10%. More disturbing was that results on the finer mesh only differed slightly from those on the coarser mesh, which indicated that even much finer meshes would be necessary for this and particularly for higher Weissenberg numbers. Indeed we observed this when we performed calculations at Weissenberg numbers of 16 and 32. A mesh with 1700 elements and a minimum length in the flow direction of $4 \times 10^{-5} R$ still overpredicted the stress coefficient λ in the wake by almost a factor of 2. The reason for this seems to be the interpolation step that is necessary to determine the initial value at the start of a fluid trajectory corresponding to a single time step. When steep gradients are present, an accurate initial value is only obtained when element sizes are very small. The simulation time for the mesh with 1700 elements was of the order of a day to reach a steady-state solution. We note in passing that these simulations are only between 2 streamlines that are close to each other. In order to get a good view of the boundary layer, a large number of such simulations between different streamlines would be necessary. In combination with the much finer meshes that would be needed to obtain a mesh converged solution (if at all possible, the stress λ was still almost a factor two off on the most refined mesh at $We = 16$), this would imply months or years of computational time. This was clearly not an option and instead we developed the Lagrangian method described in Section 3. In sharp contrast with BLPM, the computational time at $We = 16$ was only a couple of minutes for the whole flow domain.

For the validation of our technique with Mathematica we use the stress components λ, μ, and ν of [11], which evolve according to

$$\begin{aligned} We\boldsymbol{v}\cdot\nabla\nu+\nu &= \frac{|\boldsymbol{v}|^2}{We}, \\ We\boldsymbol{v}\cdot\nabla\mu+\mu &= -We\nu\nabla\cdot\boldsymbol{w}, \\ We\boldsymbol{v}\cdot\nabla\lambda+\lambda &= -2\,We\mu\nabla\cdot\boldsymbol{w}+\frac{1}{We|\boldsymbol{v}|^2}. \end{aligned} \tag{9}$$

By representing the constitutive equations in the stress components λ, μ, and ν, the system of equations becomes decoupled. First we can solve the equation for ν. Once we know ν, the equation for μ can be solved and with the obtained μ we finally solve the equation for λ.

The solution of each of these equations is obtained by integration of the right-hand sides along the streamlines,

$$\tau=\frac{1}{We}\int_0^\infty \mathrm{e}^{-s/\,We} f(\boldsymbol{z}(\boldsymbol{x},s))\;\mathrm{d}s, \tag{10}$$

where $\boldsymbol{z}(\boldsymbol{x},s)$ is a point on the same streamline as $\boldsymbol{x}$ such that the fluid takes the time s to move from $\boldsymbol{z}$ to $\boldsymbol{x}$. The function f is one of the right-hand sides in Eq. (9) and τ is the corresponding stress component ν, μ, or λ.

After computing the appropriate x and y coordinates of a streamline defined by Eq. (6) for some specified value of the stream function ψ, the 3 stress integrals are evaluated using a standard Mathematica routine (NIntegrate) for the evaluation of the integrals. Figure 3 shows a comparison of the largest stress component λ at a Weissenberg number of $We = 32$. The values of λ are taken along a streamline through the region with large stresses along the cylinder and in the wake (streamfunction value $\psi = 2.5\times10^{-4}$). Figure 3 shows that the agreement between the two numerical techniques is excellent and that both results are indistinguishable on the scale of the figures. Even the zoom around the downstream stagnation point doesn't show any noticeable difference near the local minimum and maxima. Due to excessive computational times of the Mathematica code (computing a result along 1 streamline takes at least two orders of magnitude more than the results along all streamlines for the regular C code), we have limited ourselves to $We = 32$.

For larger Weissenberg numbers, we have verified that the method converges when the time step is refined. Figure 4 shows the largest stress component λ along a trajectory in the thin high-stress region ($\log\psi = -7.330018$) for the time steps $\Delta t = 4\times10^{-4}$, $\Delta t = 2\times10^{-4}$, and $\Delta t = 10^{-4}$. Even in the zoom around the maximum value of λ, the three curves are indistinguishable at the

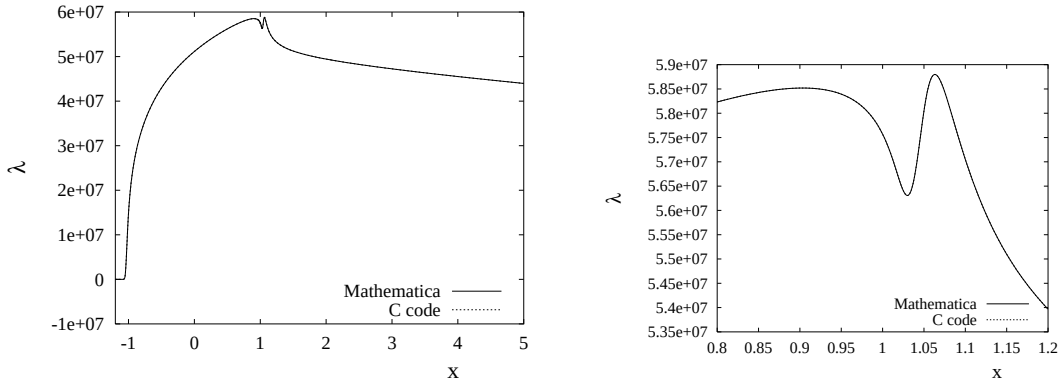

Fig. 3. Comparison between Mathematica's and our C code's results for the stress λ along the streamline with streamfunction value $\psi = 2.5 \times 10^{-4}$. Weissenberg number is $We = 32$ and the x-coordinates $-1 \leq x \leq 1$ correspond to the cylinder. (a) Around the cylinder and the start of the wake; (b) Zoom at the downstream stagnation point at $x = 1$.

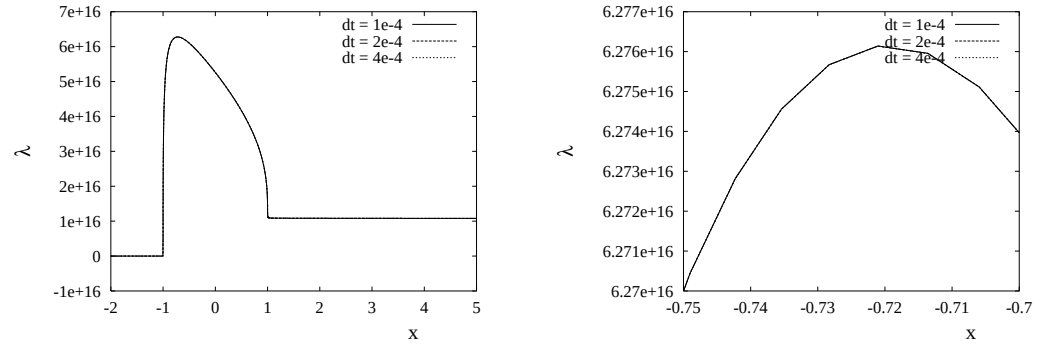

(a) (b)

Fig. 4. λ along streamline $\log \psi = -7.330018$ for $\Delta t = 4 \times 10^{-4}$, 2×10^{-4}, and 10^{-4}; (a) along the cylinder and in the wake, (b) zoom around the maximum around $x \approx -0.72$.

scale of the figure. For all results in the next sections, we used a time step of 10^{-4}.

5 Asymptotic scalings at high Weissenberg numbers

We verify the high Weissenberg number asymptotic scalings of the stress components λ and μ close to the cylinder and of λ in the wake of the cylinder. Asymptotical analysis [11] predicts that when the Weissenberg number is increased, the stress components λ and μ grow fastest in a region just outside the boundary layer and birefringent strand. It is, however, not known at which

values of the Weissenberg number the predictions are valid. For this we performed simulations for Weissenberg numbers starting from $We = 1$ up to $We = 1024$ where every consecutive Weissenberg number is taken two times as large. The boundary layer and birefringent strand occur at stream function values of the order We^{-2}, which corresponds to y-coordinate values of order We^{-1}. This will lead to very thin large-stress regions which are difficult to detect in contour plots in the xy plane. Instead, we use contour plots in the x-$\log(\psi)$ plane. In the resulting rectangular geometry a horizontal line corresponds to the values along a trajectory.

5.1 λ close to the cylinder

In the wake, asymptotical analysis predicts a maximum λ in the high stress region just outside the boundary layer. For this it is necessary that the stresses are convected around the cylinder. For the "low Weissenberg numbers" $We =$ 1, 2, or 4, this is not the case. The first Weissenberg number for which the stress λ does not completely decay is $We = 8$ as can be observed from Fig. 5. The largest values of λ are near the cylinder wall. This is not surprising since λ (not the viscoelastic stress $\boldsymbol{T}$) is singular when the velocity is zero. Another region with large values of λ starts to develop, however, at values of the stream function of $\psi \approx 10^{-3}$ to 10^{-4}. This corresponds to coordinate values $y \approx 10^{-1}$ to 10^{-2}. This is what we called the "high-stress region" just outside the boundary layer along the cylinder wall in Section 2. Relaxation is not negligible at these values of the Weissenberg numbers. The slightly larger values of λ in this region than in the boundary layer lead therefore only to a small off-centerline maximum just outside the birefringent strand in the wake.

The high-stress region along the cylinder becomes more pronounced when the Weissenberg number is increased. At Weissenberg numbers $We = 32$ and $We = 64$, λ is much larger in the high-stress region than near the edge of the boundary layer along the cylinder. Although there is some relaxation, large values of λ are convected around the cylinder. This results in a clearly observable high-stress region in the wake which we will discuss shortly. In the $x - \log(\psi)$ plots it also becomes apparent that the boundary layer and high-stress region shift towards the wall when the Weissenberg number increases. At $We = 64$ it is centered around $\psi \approx 10^{-5}$ to 10^{-6}, i.e. $y \approx 10^{-3}$. Furthermore, the width of the high-stress region, in terms of stream function values, also decreases rapidly (note here the logarithm of the stream function on the vertical axes). Combined with the rapidly increasing values of λ, this results in very large derivatives perpendicular to the fluid trajectories.

At larger values of the Weissenberg numbers all trends continue as can be observed from Fig. 6. Stresses in the high-stress region continue to grow very

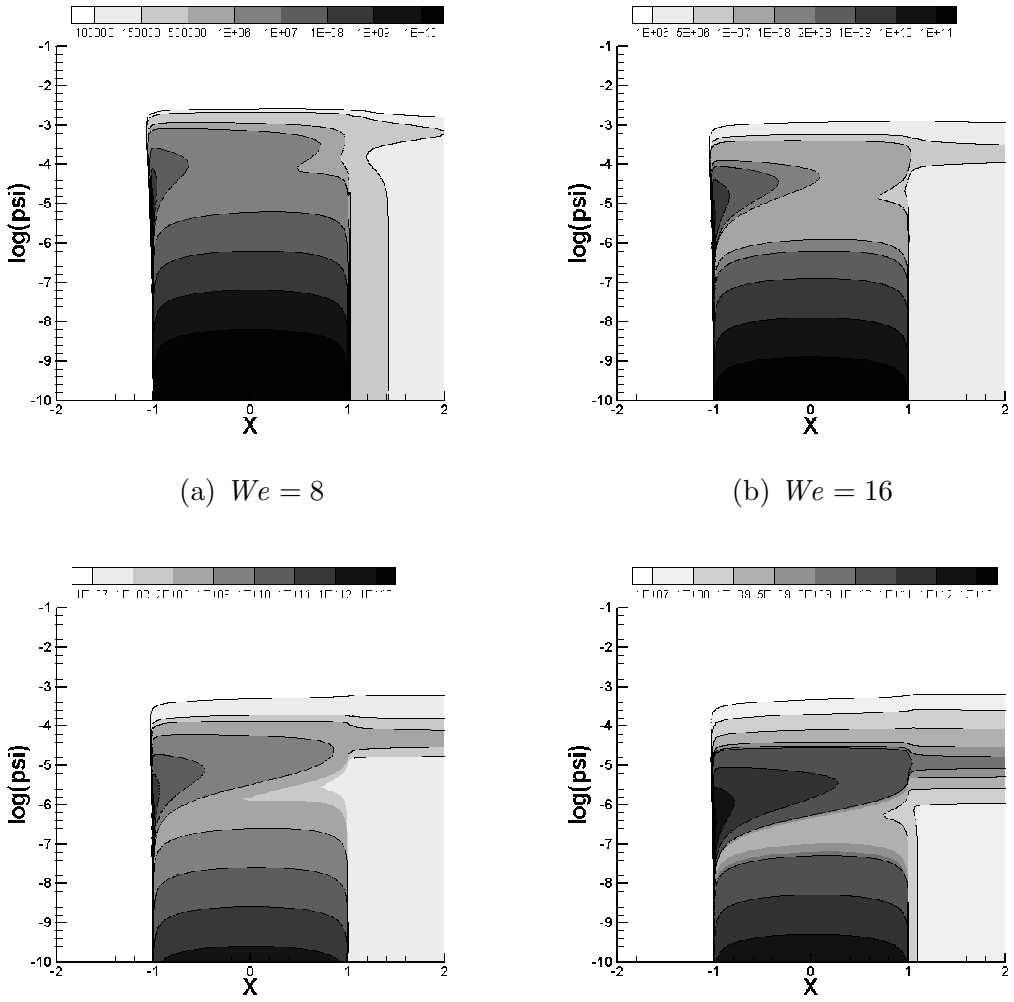

(a) $We = 8$ (b) $We = 16$

(c) $We = 32$ (d) $We = 64$

Fig. 5. Stress component λ close to cylinder and in initial part of wake for medium values of the Weissenberg number.

fast and reach values of the order of 10^{16} for the highest Weissenberg number we computed, $We = 1024$. Furthermore, the high stress region continues to move closer and closer to the cylinder wall and continues to decrease in size. At $We = 1024$, this region is at stream function values of $\psi \approx 10^{-8}$ ($y \approx 10^{-4}$) and it spans approximately the range stream function values $[10^{-6.5} - 10^{-9}]$, i.e. a width of approximately 10^{-3}. We note in passing that the stress boundary layer is no longer apparent at $We = 1024$. This is because it occurs at stream function values even lower than 10^{-10}. At $We = 128$, $We = 256$, and $We = 512$, however, the outer edge of the boundary layer is still visible.

The scalings We^k predicted in [11] and summarized in Fig. 1 are not easy to read from the figures. Therefore, we also include tables to verify the various powers k of these scalings quantitatively. Henceforth, the scaling of a quantity

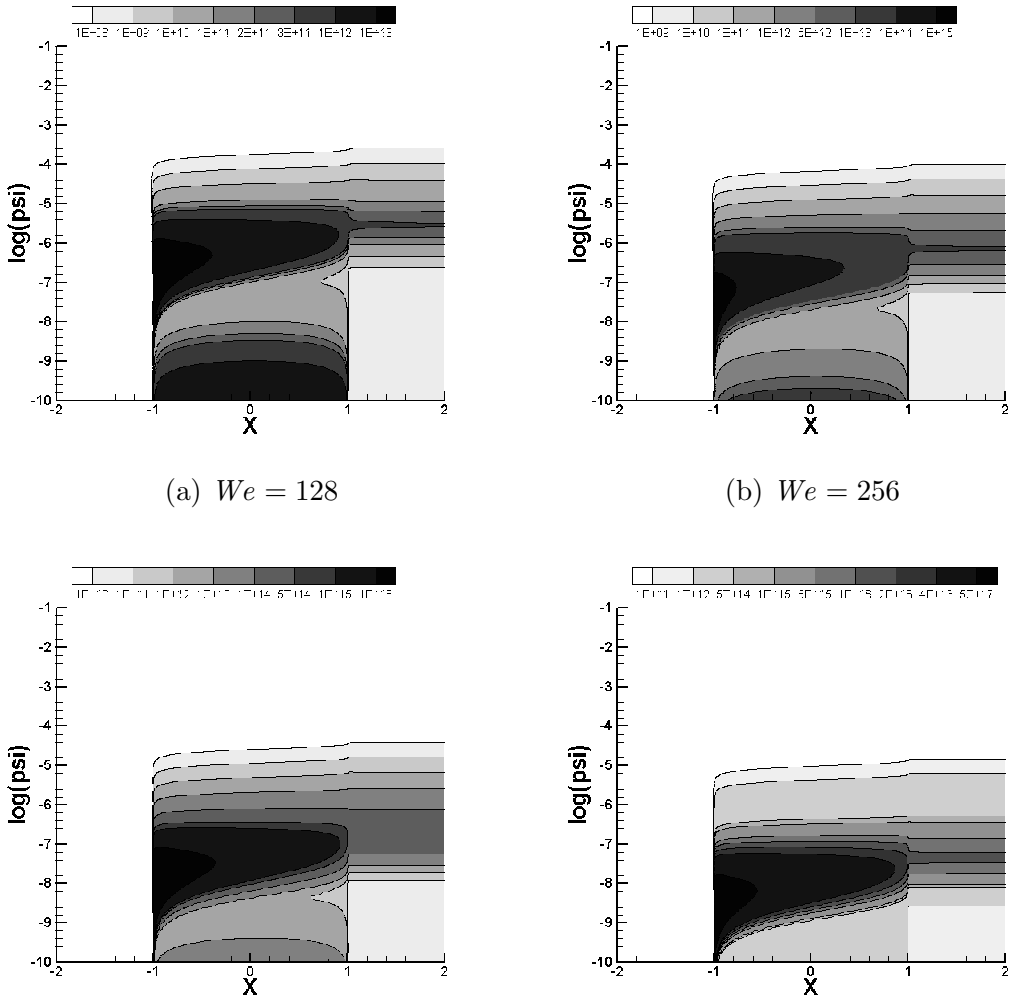

(a) $We = 128$ (b) $We = 256$

(c) $We = 512$ (d) $We = 1024$

Fig. 6. Stress component λ along cylinder and in initial part of wake for high values of the Weissenberg number.

z at a certain Weissenberg number has been computed using the ratio of the value z at this Weissenberg number and the value of z at the previous Weissenberg number. For this, no scalings are reported for the lowest values.

In the high-stress region, asymptotical analysis predicts that $\lambda \sim We^5$ and $\mu \sim We^2$. We have verified these scalings by inspecting the largest value of μ and λ in the high stress region at the cross section $x = 0$, i.e. above the top of the cylinder.

Table 2 contains the scalings for the maximum λ in the high-stress region and in the cross section at $x = 0$ together with the stream function value at which this maximum occurs. It appears that the scalings approach the asymptotical scalings from above. At the lower values of We the agreement is already fairly

We	λ	scaling	ψ	scaling
8	$2.86 \cdot 10^{6}$		$2.68 \cdot 10^{-4}$	
16	$1.13 \cdot 10^{8}$	5.30	$5.44 \cdot 10^{-5}$	-2.30
32	$4.29 \cdot 10^{9}$	5.25	$1.13 \cdot 10^{-5}$	-1.96
64	$1.50 \cdot 10^{11}$	5.13	$2.91 \cdot 10^{-6}$	-1.96
128	$5.06 \cdot 10^{12}$	5.08	$7.46 \cdot 10^{-7}$	-1.96
256	$1.66 \cdot 10^{14}$	5.04	$1.91 \cdot 10^{-7}$	-1.97
512	$5.40 \cdot 10^{15}$	5.02	$4.68 \cdot 10^{-8}$	-2.03
1024	$1.74 \cdot 10^{17}$	5.01	$1.19 \cdot 10^{-8}$	-1.98

Table 2
Scalings for λ in the high-stress region along the cylinder: maximum value of λ at cross section $x = 0$, scaling of λ with Weissenberg number, stream function value ψ corresponding to maximum λ, and scaling of ψ with Weissenberg number.

good. For the highest values of We, the agreement with the asymptotic results ($k = 5$) is excellent. Additionally, the scaling of the stream function values at which these maxima appear correspond with the asymptotical value $k = -2$. We remark in passing that the maximum values of λ appear at lower stream function values than the maximum values of μ.

The local minima of λ at $x = 0$ close to the cylinder are given in Table 3.

We	λ	scaling	ψ	scaling
8	$1.45 \cdot 10^{6}$		$4.34 \cdot 10^{-5}$	
16	$1.79 \cdot 10^{7}$	3.63	$7.01 \cdot 10^{-6}$	-2.63
32	$1.90 \cdot 10^{8}$	3.41	$1.47 \cdot 10^{-6}$	-2.29
64	$1.94 \cdot 10^{9}$	3.35	$3.01 \cdot 10^{-7}$	-2.29
128	$1.88 \cdot 10^{10}$	3.28	$6.14 \cdot 10^{-8}$	-2.29
256	$1.75 \cdot 10^{11}$	3.22	$1.19 \cdot 10^{-8}$	-2.37
512	$1.67 \cdot 10^{12}$	3.25	$2.42 \cdot 10^{-9}$	-2.30
1024	$1.54 \cdot 10^{13}$	3.21	$6.18 \cdot 10^{-10}$	-1.97

Table 3
Scaling of λ in the boundary layer along the cylinder: local minimum value of λ at cross section $x = 0$, scaling of λ with Weissenberg number, stream function value ψ corresponding to minimum λ, and scaling of ψ with Weissenberg number.

Close to the cylinder, asymptotical analysis predicts that μ is of order unity in the boundary layer along the cylinder and scales as We^2 in the high-stress region just outside the boundary layer. The contour plots corresponding to the four largest Weissenberg numbers are displayed in Fig. 7. Indeed, in the

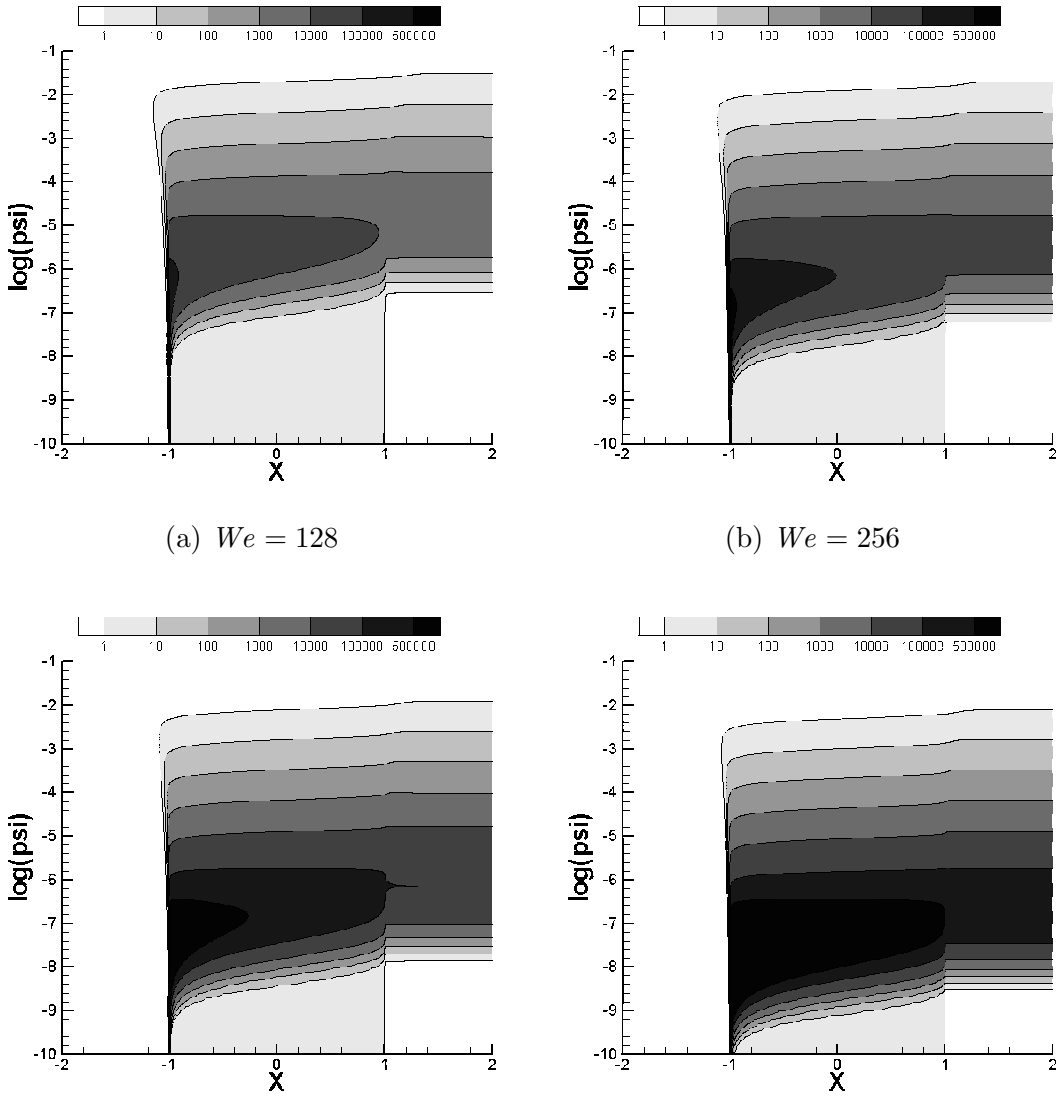

(a) $We = 128$ (b) $We = 256$

(c) $We = 512$ (d) $We = 1024$

Fig. 7. Stress component μ along cylinder and in early stages of the wake for various values of the Weissenberg number.

boundary layer along the cylinder the value of μ is of order unity, smaller than 10, and does not seem to change when the Weissenberg number is increased. In a region just outside the boundary layer, μ does increase with increasing

Weissenberg number, although considerably slower than λ. As for λ, this region shifts towards the cylinder as We increases, but the maximum seems to occur at slightly larger values of the stream function. As for λ, the derivative along the streamlines is very large near the upstream stagnation point and the large values of μ continue into the wake where they decay to the equilibrium value.

To verify the scaling in the boundary layer and in the high-stress region we examine the values of μ in the cross section $x = 0$. The value of μ at $x = 0$ at the streamline closest to the cylinder are given in Table 4. For all Weissenberg

We	μ	scaling
8	8.00	
16	8.00	0.00
32	7.99	0.00
64	7.98	0.00
128	7.94	-0.01
256	7.76	-0.03
512	7.99	0.04
1024	7.96	-0.01

Table 4
Scaling of μ in the boundary layer along the cylinder: value of μ at streamline closest to cylinder at cross section $x = 0$ and scaling of μ with Weissenberg number.

numbers, $\mu \approx 8$ in the boundary layer along the cylinder. The predicted scaling We^0 is already valid for the lowest Weissenberg numbers considered here.

In order to verify the scalings in the high-stress region, we examine the maximum in the cross section at $x = 0$. Table 5 contains the scalings for μ together with the stream function value at which this maximum occurs. At the lower Weissenberg numbers, the scaling is slightly higher than the theoretical value of $k = 2$, but for the largest Weissenberg numbers we find excellent agreement. Additionally, the scaling of the stream function values at which these maxima appear correspond with the asymptotical value $k = -2$.

5.3 λ in the wake of the cylinder

In order to observe the high Weissenberg number scalings for the wake, the stress components need to be convected completely around the cylinder. If this is the case, asymptotical analysis [11] predicts that λ is proportional to We^5 in a thin region just outside the birefringent strand where λ scales as We^3. When discussing the scaling of λ along the cylinder wall, we observed

We	μ	scaling	ψ	scaling
8	$5.95 \cdot 10^{1}$		$8.37 \cdot 10^{-4}$	
16	$2.89 \cdot 10^{2}$	2.28	$2.13 \cdot 10^{-4}$	-1.97
32	$1.33 \cdot 10^{3}$	2.20	$4.44 \cdot 10^{-5}$	-2.26
64	$5.77 \cdot 10^{3}$	2.12	$1.13 \cdot 10^{-5}$	-1.97
128	$2.42 \cdot 10^{4}$	2.07	$2.91 \cdot 10^{-6}$	-1.96
256	$9.93 \cdot 10^{4}$	2.04	$7.46 \cdot 10^{-7}$	-1.96
512	$4.03 \cdot 10^{5}$	2.02	$1.83 \cdot 10^{-7}$	-2.03
1024	$1.60 \cdot 10^{6}$	1.99	$3.72 \cdot 10^{-8}$	-2.29

Table 5
Scalings for μ in the high-stress region along the cylinder: maximum value of μ in high stress region at cross section $x = 0$, scaling of μ with Weissenberg number, stream function value ψ corresponding to maximum μ, and scaling of ψ with Weissenberg number.

already that the stresses did not completely decay for $We \approx 8$. Here we focus mainly on the high stress region in the wake.

Figure 8 shows that at the lowest Weissenberg number of 8, stresses are not completely convected around the cylinder and only a minor off-centerline maximum appears at stream function values of $\psi \approx 10^{-3}$. From a Weissenberg number of 16 on, a significant part of the large values of λ along the cylinder are convected around the cylinder and the high-stress region just outside the birefringent strand becomes clearly visible. For these medium values of the Weissenberg number, λ decays rather quickly in the wake. However, due to the very large values of λ this regions extends far downstream and will only approach its equilibrium value far outside the computational domain. For increasing Weissenberg numbers, the high-stress region decreases in width and shifts towards the centerline, similarly to the behaviour of λ close to the cylinder.

Figure 9 shows the birefringent strand and high-stress region for λ in the wake at Weissenberg numbers 128 to 1024. We observe that λ continues to increase rapidly and the high-stress region becomes thinner and shifts further towards the axis of symmetry. Since the magnitude of the velocity is one in this region, the viscoelastic stress T_{xx} has the same scaling as λ. This results in enormous stress derivatives in the direction perpendicular to the fluid trajectories. We note in passing that the high values of λ along the cylinder are convected far downstream. The contour lines are nearly horizontal over the computational range which is 49 radii behind the cylinder.

In order to verify the asymptotical scalings quantitatively, we examined the

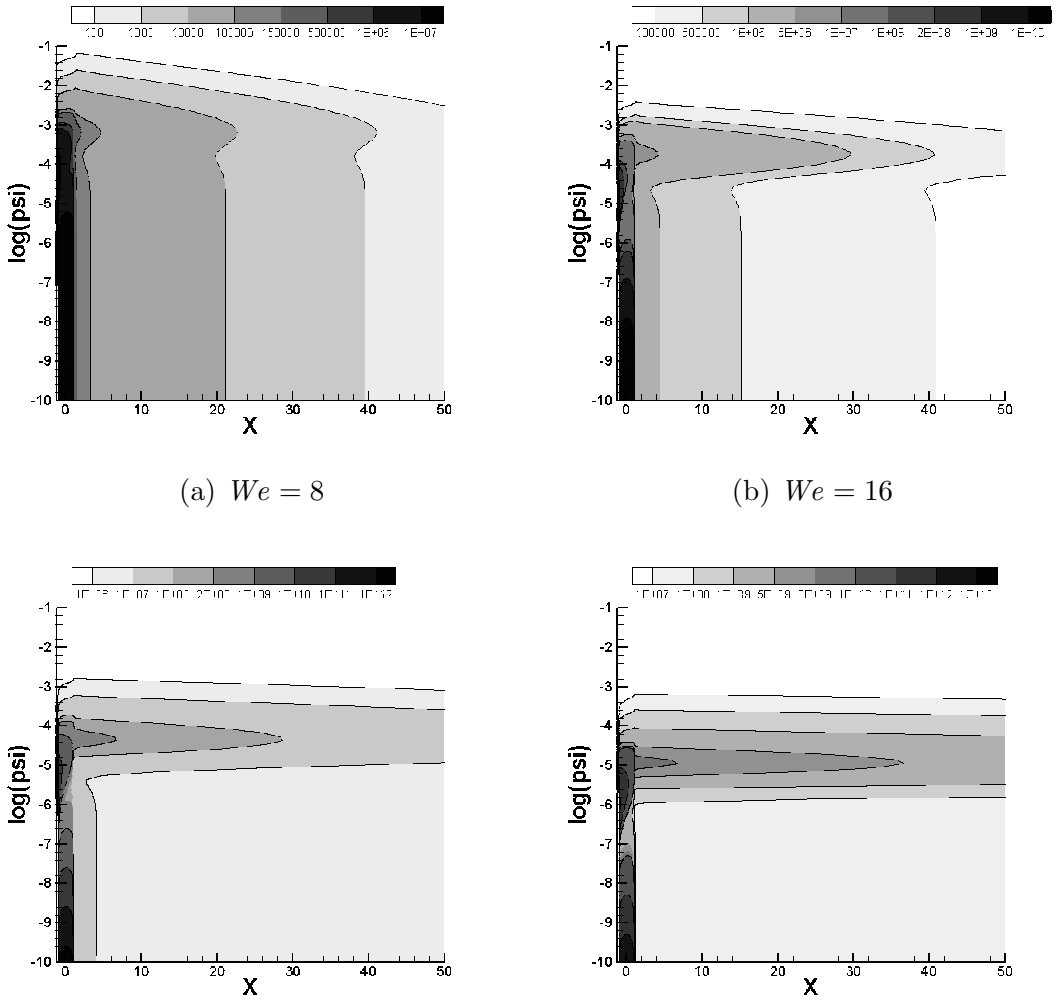

(a) $We = 8$ (b) $We = 16$

(c) $We = 32$ (d) $We = 64$

Fig. 8. Stress component λ in the wake for moderate values of the Weissenberg number.

values of λ at the cross section $x = 10$ in the wake. Table 6 displays the values of λ at $x = 10$ at the streamline closest to the centerline. At the smaller Weissenberg numbers, the scaling is considerably larger than $k = 3$. From $We = 128$ on, however, the scaling is approximately cubic and it slowly approaches $k = 3$ when We is increased further.

The maximum values of λ at $x = 10$ in the high-stress region are given in Table 7. At the lower values of the Weissenberg number, the scaling is again considerably larger than the theoretical value $k = 5$. This is because λ is only partially convected around the cylinder at those values of the Weissenberg number. Then the part that is convected around the cylinder will be considerably higher at the next Weissenberg number and result in higher values of k. From $We \approx 128$ on, however, the scaling is very close to the asymptotical

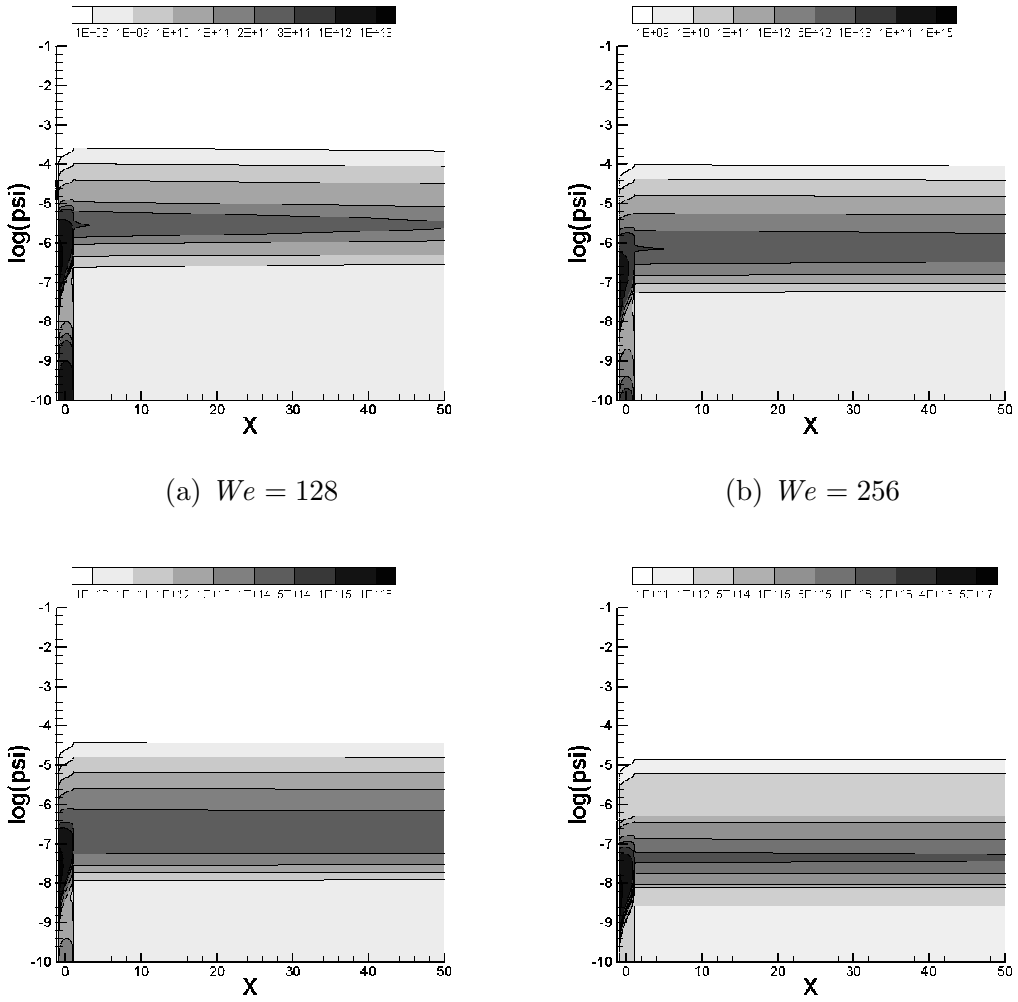

(a) $We = 128$ (b) $We = 256$

(c) $We = 512$ (d) $We = 1024$

Fig. 9. Stress component λ in wake for large values of the Weissenberg number.

value and it slowly approaches $k = 5$ when We is increased further.

6 Conclusions and discussion

In this paper, we have developed a numerical technique that is able to compute thin stress boundary layers that occur in steady viscoelastic fluid flows around a confined cylinder. The technique is both very efficient and accurate and no severe numerical problems were observed in resolving extremely thin stress boundary layers at any of the Weissenberg numbers that we used. This is in sharp contrast with one of the currently used numerical techniques in viscoelastic fluid flow, the backward-tracking Lagrangian particle method. Even in a narrow region between two streamlines, the method had severe problems

We	λ	scaling
8	$4.08 \cdot 10^4$	
16	$6.93 \cdot 10^5$	4.09
32	$8.22 \cdot 10^6$	3.57
64	$8.07 \cdot 10^7$	3.30
128	$7.18 \cdot 10^8$	3.15
256	$6.06 \cdot 10^9$	3.08
512	$5.00 \cdot 10^{10}$	3.04
1024	$4.06 \cdot 10^{11}$	3.02

Table 6
Scaling of λ in birefringent strand in the wake: λ in the cross section at $x = 10$ for the streamline closest to the centerline and scaling of λ with Weissenberg number.

We	λ	scaling	ψ	scaling
8	$4.95 \cdot 10^4$		$6.67 \cdot 10^{-4}$	
16	$3.43 \cdot 10^6$	6.11	$1.70 \cdot 10^{-4}$	-1.97
32	$1.80 \cdot 10^8$	5.71	$4.44 \cdot 10^{-5}$	-1.94
64	$7.62 \cdot 10^9$	5.40	$1.13 \cdot 10^{-5}$	-1.97
128	$2.84 \cdot 10^{11}$	5.22	$2.91 \cdot 10^{-6}$	-1.96
256	$9.83 \cdot 10^{12}$	5.11	$7.46 \cdot 10^{-7}$	-1.96
512	$3.28 \cdot 10^{14}$	5.06	$1.83 \cdot 10^{-7}$	-2.03
1024	$1.07 \cdot 10^{16}$	5.03	$4.68 \cdot 10^{-8}$	-1.97

Table 7
Scaling of λ in high-stress region in the wake: maximum λ in high-stress region in the cross section at $x = 10$, scaling of λ with Weissenberg number, stream function value ψ corresponding to maximum λ, and scaling of ψ with Weissenberg number.

in predicting the correct stresses for the lowest Weissenberg number we considered. At higher values of We, these problems increased and even meshes with a minimum element size of 4×10^{-5} showed stresses that were off by a factor of two. The main reason seemed to be the interpolation step required in BLPM to determine suitable initial values at the starting point of a fluid trajectory. Only for very refined meshes the biquadratic interpolation that we used seemed to be sufficiently accurate when very steep gradients are present. Additionally, these simulations required already significant computation times of the order of one day for just a narrow region. For the Lagrangian technique we developed, such problems were absent. No critical Weissenberg number was encountered at which the method would have convergence problems. Additionally, computation times reduced from one day for a narrow region to a

couple of minutes for the whole flow domain. In view of these results for a fixed Newtonian-like velocity field, it would not at all be surprising if solutions do exist at Weissenberg numbers larger than unity for the UCM and Oldroyd-B model and that current numerical techniques are simply not able to resolve such thin boundary layers. Even the very fine meshes used in [6] with a smallest element size of the order of 10^{-3} near the rear stagnation points could very well be too coarse.

The new method is able to predict the theoretical scalings [11] for the stresses in the flow around the cylinder using a fixed velocity field. In our numerical simulations we could indeed observe the high-stress regions just outside the boundary layer along the cylinder and birefringent strand in the wake. Along the cylinder, we also found numerically that in the boundary layer the stress component λ is proportional to We^3, while μ remains of order unity. In a thin region just outside this boundary layer the stress components λ and μ grow much faster indeed. There λ is proportional to We^5 and μ to We^2. The scalings for the stress components μ and λ are already close to the theoretical values for the relatively low Weissenberg number $We \approx 16$. At $We = 1024$, the largest value of the Weissenberg number we considered, the agreement is excellent.

To observe the theoretical scalings in the wake, the stresses need to be convected around the cylinder. For which values of Weissenberg numbers this occurs cannot be established from the asymptotical analysis. We found numerically that the first Weissenberg number for which the stress component λ does not decay completely along the the cylinder is $We = 8$. To observe a good agreement with the theoretical scalings, the Weissenberg number needs to be considerably larger, $We \approx 128$. At the largest Weissenberg number $We = 1024$, our numerical results showed again excellent agreement with the theoretical scalings $\lambda \sim We^3$ in the birefringent strand and $\lambda \sim We^5$ in the high-stress region just outside the birefringent strand. It is obvious that these scalings cannot be observed for Weissenberg numbers of order unity that can currently be attained in the benchmark flow around a cylinder using non-fixed kinematics. For such values of the Weissenberg number, stresses are simply not convected around the cylinder and the asymptotical analysis is not valid. A comparison with the asymptotical scalings in the coupled flow problem as in [5,6] is therefore useless. The scalings can only be observed at Weissenberg numbers that are one to two orders of magnitude higher, far beyond the physical applicability of the UCM and Oldroyd-B model. Alves et al. [5] claim that they observe the We^5 scaling in the wake at Weissenberg numbers of order unity. This is very curious indeed and certainly not related to the asymptotical scalings of [11].

All simulations have been performed with a Newtonian-like velocity field that fulfills the essential requirements near the cylinder. Such an analytical expres-

sion facilitates comparison of numerical techniques for computing viscoelastic stresses. Interestingly, the scalings of the viscoelastic stress components were obtained nearly exactly using a relatively crude approximation to the Newtonian velocity field. Apparently the scalings are not very sensitive to small changes in the kinematics. This would suggest that it could be most important to compute the viscoelastic stresses very precisely when the equations of motion are included. A less accurate approximation of the kinematics could be sufficient.

Compared to the benchmark flow around a cylinder with non-fixed kinematics, numerical simulation in a fixed, Newtonian-like velocity field is easier since the equations of motion do not need to be solved. The velocity field could also be different from a Newtonian velocity field. However, in the vicinity of the cylinder and in the wake, where large stresses develop, the Newtonian-like velocity field is qualitatively similar to the velocity field obtained for an Oldroyd-B fluid at a Weissenberg number close to the limiting Weissenberg number of order unity. As for the coupled flow problem, simulations using a Newtonian-like velocity field are far from easy since thin regions with large stresses exist. Although there will be quantitative differences in the stress fields, both problems share the main difficulty concerning the numerical computation of the stress field: thin regions with large stresses near the cylinder wall and the plane of symmetry in the wake. The key advantage of the fixed-kinematics flow around a cylinder is that a unique solution does exist for any Weissenberg number. This makes the flow of a UCM fluid around a cylinder using the fixed Newtonian like velocity field a very good benchmark problem to test state-of-the-art numerical techniques for viscoelastic flow computations. If a numerical technique with corresponding mesh fails to converge for the fixed kinematics case, one can be certain that this is caused by the numerics. Additionally, such methods will off course fail to resolve similar stress boundary layers in the (harder) coupled flow problem. The correct stresses in the stress boundary layers can be obtained relatively easily with the Lagrangian numerical technique that we developed. This opens the possibility to establish whether a certain numerical technique, with a corresponding mesh, is able to accurately resolve the thin stress boundary layers. If a method introduces too much artificial diffusion, this can easily be detected. Before trying the coupled flow problem, it would be a good idea if the fixed kinematics flow around a cylinder is tried first to evaluate the numerical scheme used to resolve the viscoelastic stresses. Furthermore, improvement and analyzing why a numerical scheme fails is much easier in this case.

Now we have developed a numerical technique that can resolve thin stress boundary layers in the flow around a cylinder with fixed kinematics, the main challenge is to develop a numerical framework that can handle the coupled flow problem. At Weissenberg numbers of the order unity at which current numerical methods fail for the coupled flow problem, two possible solution

techniques are eminent. First, one could use BLPM but then every fluid trajectory needs to be integrated backwards in time until it reaches a region upstream where the configuration tensor is sufficiently smooth. This will minimize the impact of interpolation errors in regions with steep stress gradients which occur when the fluid motion is only tracked a single time step backwards in time. For the cylinder problem, this means that for streamlines that pass far enough from the cylinder, integrating one single time step backwards in time will probably be sufficient since no steep stress gradients develop in these regions. For every location close to the cylinder surface and plane of symmetry in the wake, however, the fluid motion has to be tracked up to a region upstream of the cylinder where no large stresses are present. This will lead to a significant increase in the computational cost since many of the locations where stresses needs to be computed lie in these regions with steep stress gradients. Parallelization is indispensable in this case. A second option would be to use the purely Lagrangian technique in combination with, for example, a finite element technique where elements are oriented along the fluid trajectories. Although this requires some significant changes in the equations of motion, the efficient and accurate stress computations of the purely Lagrangian scheme are retained and any interpolation of stresses or configuration tensors is explicitly avoided. Parallelization will not be necessary at Weissenberg numbers of unity. Of course, the coupled flow problem also introduces other issues such as the nonlinear coupling between the equations of motion and the constitutive equations. Whether this leads to severe numerical problems when stress boundary layers are resolved remains to be established.

The numerical technique we developed to integrate the stress equations can also be useful for research groups that use other numerical techniques to simulate the flow around a cylinder or similar viscoelastic flow problems with thin stress boundary layers. First, it can be used to establish an appropriate mesh which is able to resolve the stress boundary layers at a given Weissenberg number. Second, and more important, the Lagrangian technique can also be used a posteriori to compute the correct stress field for the resulting steady state velocity field of the coupled flow problem. In this way one can establish whether thin stress boundary layers have been resolved properly. In case the stresses in the wake do not converge or are inaccurate at very fine meshes, the Lagrangian technique can be used to compute the correct stress fields which can be used to analyze why the numerics fail. Of course, such an analysis is not restricted to the UCM or Oldroyd-B model, but can equally well be applied to more realistic viscoelastic models which show thin stress boundary layers as well.

References

[1] A. W. Liu, D. E. Bornside, R. C. Armstrong, R. A. Brown, Viscoelastic flow of polymer solutions around a periodic, linear array of cylinders: comparisons of predicitons for microstructure and flow fields, J. Non-Newtonian Fluid Mech. 77 (1998) 153–190.

[2] Y. R. Fan, R. I. Tanner, N. Phan-Thien, Galerkin/least-square finite-element methods for steady viscoelastic flows, J. Non-Newtonian Fluid Mech. 84 (1999) 233–256.

[3] J. Sun, M. D. Smith, R. C. Armstrong, R. A. Brown, Finite element method for viscoelastic flows based on the discrete adaptive viscoelastic stress splitting and the discontinuous Galerkin method: DAVSS-G/DG, J. Non-Newtonian Fluid Mech. 86 (1999) 281–307.

[4] H.-S. Dou, N. Phan-Thien, The flow of an Oldroyd-B fluid past a cylinder in a channel: adaptive viscosity vorticity (DAVSS-ω) formulation, J. Non-Newtonian Fluid Mech. 87 (1999) 47–73.

[5] M. A. Alves, F. T. Pinho, P. J. Oliveira, The flow of viscoelastic fluids past a cylinder: finite-volume high-resolution methods, J. Non-Newtonian Fluid Mech. 97 (2001) 207–232.

[6] A. E. Caola, Y. L. Yoo, R. C. Armstrong, R. A. Brown, Highly parallel time integration of viscoelastic flows, J. Non-Newtonian Fluid Mech. 100 (2001) 191–216.

[7] C. Chauvière, R. G. Owens, A new spectral element method for the reliable computation of viscoelastic flow, Comp. Meth. Appl. Mech. Eng. 190 (2001) 3999–4018.

[8] R. G. Owens, C. Chauvière, T. N. Phillips, A locally-upwinded spectral technique (LUST) for viscoelastic flows, J. Non-Newtonian Fluid Mech. 108 (2002) 49–71.

[9] R. G. Owens, T. N. Phillips, Computational Rheology, Imperial College Press, London, 2002.

[10] F. P. T. Baaijens, S. H. A. Selen, H. P. W. Baaijens, G. W. M. Peters, H. E. H. Meijer, Viscoelastic flow past a confined cylinder of a low density polyethylene melt, J. Non-Newtonian Fluid Mech. 68 (1997) 173–203.

[11] M. Renardy, Asymptotic structure of the stress field in flow past a cylinder at high Weissenberg number, J. Non-Newtonian Fluid Mech. 90 (2000) 13–23.

[12] P. Halin, G. Lielens, R. Keunings, V. Legat, The Lagrangian particle method for macroscopic and micro-macro viscoelastic flow computations, J. Non-Newtonian Fluid Mech. 79 (1998) 387–403.

[13] P. Wapperom, R. Keunings, V. Legat, The backward-tracking Lagrangian particle method (BLPM) for transient viscoelastic flows, J. Non-Newtonian Fluid Mech. 91 (2000) 273–295.

[14] M. A. Hulsen, J. P. P. M. van der Zanden, Mathematical and physical requirements for successful computations with viscoelastic fluid models, J. Non-Newtonian Fluid Mech. 29 (1988) 93–117.

[15] P. Wapperom, A simple transformation to guarantee positive definiteness of the configuration tensor in two-dimensional numerical calculations In preparation.